Intelligent Omni-Surfaces: Ubiquitous Wireless Transmission by Reflective-Refractive Metasurfaces

Shuhang Zhang, *Student Member, IEEE*, Hongliang Zhang, *Member, IEEE*, Boya Di, *Member, IEEE*, Yunhua Tan, Marco Di Renzo, *Fellow, IEEE*, Zhu Han, *Fellow, IEEE*, H. Vincent Poor, *Life Fellow, IEEE*, and Lingyang Song, *Fellow, IEEE*

***Abstract*— Intelligent reflecting surfaces (IRSs), which are capable of adjusting radio propagation conditions by controlling the phase shifts of the waves that impinge on the surface, have been widely analyzed for enhancing the performance of wireless systems. However, the reflective properties of widely studied IRSs restrict the service coverage to only one side of the surface. In this paper, to extend the wireless coverage of communication systems, we introduce the concept of intelligent omni-surface (IOS)-assisted communication. More precisely, an IOS is an important instance of a reconfigurable intelligent surface (RIS) that can provide service coverage to mobile users (MUs) in a reflective and a refractive manner. We consider a downlink IOS-assisted communication system, where a multi-antenna small base station (SBS) and an IOS jointly perform beamforming, for improving the received power of multiple MUs on both sides of the IOS, through different reflective/refractive channels. To maximize the sum-rate, we formulate a joint IOS phase shift design and SBS beamforming optimization problem, and propose an iterative algorithm to efficiently solve the resulting non-convex program. Both theoretical analysis and simulation results show that an IOS significantly extends the service coverage of the SBS when compared to an IRS.**

***Index Terms*— Intelligent omni-surface, phase shift design, analog and digital beamforming.**

Manuscript received October 20, 2020; revised March 28, 2021 and June 24, 2021; accepted June 25, 2021. Date of publication July 20, 2021; date of current version January 10, 2022. This work was supported in part by the National Natural Science Foundation of China under Grant 61931019, Grant 61625101, Grant 61829101, and Grant 61941101 and in part by the U.S. National Science Foundation under Grant EARS-1839818, Grant CNS-1717454, Grant CNS-1731424, Grant CNS-1702850, and Grant CCF-1908308. The work of Marco Di Renzo was supported in part by the European Commission through the H2020 ARIADNE Project under Grant 871464 and through the H2020 RISE-6G Project under Grant 101017011. The associate editor coordinating the review of this article and approving it for publication was C. Masouros. *(Corresponding author: Lingyang Song.)*

Shuhang Zhang, Boya Di, Yunhua Tan, and Lingyang Song are with the Department of Electronics, Peking University, Beijing 100871, China (e-mail: shuhangzhang@pku.edu.cn; diboya@pku.edu.cn; tanggeric@pku.edu.cn; lingyang.song@pku.edu.cn).

Hongliang Zhang and H. Vincent Poor are with the Department of Electrical and Computer Engineering, Princeton University, Princeton, NJ 08544 USA (e-mail: hongliang.zhang92@gmail.com; poor@princeton.edu).

Marco Di Renzo is with Université Paris-Saclay, CNRS, CentraleSupélec, Laboratoire des Signaux et Systèmes, 91192 Gif-sur-Yvette, France (e-mail: marco.di-renzo@universite-paris-saclay.fr).

Zhu Han is with the Department of Electrical and Computer Engineering, University of Houston, Houston, TX 77004 USA, and also with the Department of Computer Science and Engineering, Kyung Hee University, Seoul 02447, South Korea (e-mail: hanzhu22@gmail.com).

Color versions of one or more figures in this article are available at https://doi.org/10.1109/TWC.2021.3094869.

Digital Object Identifier 10.1109/TWC.2021.3094869

I. Introduction

THE explosive growth of the number of mobile devices has brought new user requirements and applications, and innovative networking characteristics for future communications [1], [2], which necessitate radically novel communication paradigms [3]. During the past few years, there has been a growing interest in developing new transmission technologies for exploiting the implicit randomness of the propagation environment, so as to provide high-speed and seamless data services [4], [5], such as spatial modulation [6] and massive multiple-input and multiple-output (MIMO) technologies [7]. However, the implementation of massive MIMO is still constrained by implementation bottlenecks, which include the hardware cost, the total energy consumption, and the high complexity for signal processing [8], [9]. Due to these complexity constraints, therefore, the quality of service (QoS) is not always guaranteed in harsh propagation environments [10].

The recent development of metasurfaces has motivated the introduction of a new hardware technology for application to wireless communications, i.e., the reconfigurable intelligent surface (RIS) [11], [12], which can improve the spectral efficiency, the energy efficiency, the security, and the communication reliability of wireless networks [13], [14]. An RIS is an ultra-thin surface containing multiple sub-wavelength nearly-passive scattering elements [15]. The sub-wavelength separation between adjacent elements of the RIS enables exotic manipulations of the signals impinging upon the surface [16], [17]. A typical implementation of an RIS consists of many passive elements that can control the electromagnetic responses of the signals through the appropriate configuration of positive intrinsic negative (PIN) diodes distributed throughout the surface [18], [19]. Depending on the ON/OFF status of the PIN diodes, several signal transformations can be applied [20]. The programmable characteristics of the RIS enables it to shape the propagation environment as desired [21], and allows for the re-transmission of signals to the receiver at a reduced cost, size, weight, and power [22], [23].

In the literature, a widely studied example of RIS is referred to as an intelligent reflecting surface (IRS), in which the metasurface is designed for reflecting the signals impinging upon one side of the surface towards users located on the same side of the surface [24]. The feasibility of transmitting and receiving signals with IRSs in wireless communication

systems has been verified in [25] and [26]. Based on such capabilities, studies of IRS-aided transmission include the following. In [27], a joint power allocation and continuous phase shift design is studied for application to a reflective IRS-assisted system in order to maximize the energy efficiency. In [28], the achievable data rate of a reflective IRS-assisted communication system is evaluated and the effect of a limited number of phase shifts on the data rate is investigated. In [29], the IRS beamforming and phase shift designs are jointly optimized to maximize the sum-rate in a reflective IRS-assisted point-to-point communication system. In [30], a reflective IRS is deployed at the cell boundary of multiple cells to assist the downlink transmission of cell-edge users, whilst mitigating the inter-cell interference.

In these studies, as mentioned, signals that impinge upon one of the two sides of the surface are completely reflected towards the same side. This implies that users located on the opposite side of the surface cannot be served by an IRS: They are out of coverage. To tackle this issue, we introduce an intelligent omni-surface (IOS)-assisted communication system. The proposed IOS is deployed in a general multi-user downlink communication system and, in contrast with an IRS, it has the dual functionality of signal reflection and refraction [31]. More precisely, signals impinging upon one of either side of the IOS can be simultaneously reflected and refracted towards mobile users (MUs) that are located on the same side and the opposite side of the IOS, respectively [32]. Similar to an IRS, an IOS is made of multiple passive scattering elements and programmable PIN diodes, which are appropriately designed and configured, respectively, to customize the propagation environment [33]. Unlike an IRS that completely reflects all the incident signals, an IOS is capable of simultaneously reflecting and refracting the incident signals [34]. The power ratio of the refracted and reflected signals is determined by the hardware structure of the IOS [35]. By enabling joint reflection and refraction, an IOS provides ubiquitous wireless coverage to the MUs on both of its sides, and the propagation environment of all the users can be jointly customized by adjusting the phase shifts of the IOS scattering elements [36]. As a result, the power of the received signals can be enhanced, and the QoS of the communication links can be improved.

To serve the MUs with good performance, it is of vital importance to design the amplitude and phase response of the passive scatterers of the IOS. As mentioned in [37], the optimization of an IRS-aided system can be viewed as a joint analog beamforming design at the RIS and a digital beamforming design at the base station (BS), with the objective of shaping the propagation environment and improving the sum-rate of the network. In an IOS-assisted communication system, the analog beamforming performed at the IOS and the digital beamforming performed at the BS provide directional reflective/refractive radio waves to the MUs on both sides of the IOS concurrently.

However, when compared to an IRS-assisted communication system [37], the analog and digital beamforming design of an IOS-assisted communication system faces several new challenges. *First*, the power of the reflected and refracted signals of the IOS may not be symmetric, i.e., the channel model of the reflected and refracted signals can be different [32]. Therefore, the methods developed and the results obtained for IRSs may not be applicable to an IOS-assisted communication system. *Second*, the power ratio of the reflected and refracted signals of an IOS can be appropriately optimized, which provides an extra degree of freedom for enhancing the communication performance [31]. In particular, the interplay between the spatial distribution of the MUs and the optimal power ratio of the reflected and refracted signals plays an important role. *Third*, the line-of-sight (LoS) transmission link from the BS to the MUs may exist concurrently with the signals that are reflected and refracted from the IOS, which implies that the IOS needs to be optimized in order to account for the LoS links as well.

In this paper, motivated by these considerations, we aim to jointly optimize the digital beamforming at the BS and the analog reflective+refractive beamforming at the IOS, in order to maximize the sum-rate of an IOS-assisted communication system. The main contributions of this paper can be summarized as follows.

1) We propose a multi-user IOS-assisted downlink communication system, where an IOS is deployed to improve the QoS of several MUs that are located on both sides of the IOS. The physical characteristics of the IOS and the channel setup of the considered system model are introduced and discussed.
2) A joint BS digital beamforming and IOS analog reflective+refractive beamforming design problem is formulated to maximize the sum-rate of the MUs on both sides of the IOS. The NP-hard problem is decoupled into two subproblems: digital beamforming optimization and analog beamforming optimization, which are solved iteratively.
3) We analyze the performance of the IOS-assisted downlink communication system theoretically. The data rate gain of the MUs on different locations is derived, and the optimal power ratio of the reflected and refracted signals with respect to the spatial distribution of the MUs is computed.
4) Simulation results verify the theoretical performance of the proposed multi-user IOS-assisted downlink communication system. The numerical results reveal that the IOS significantly improves the data rate of the MUs on both of its sides concurrently, when compared to the cellular system.

The rest of this paper is organized as follows. In Section II, we introduce the structure and properties of the IOS. In Section III, we illustrate the considered multi-user IOS-assisted downlink communication system, including the channel model and the beamforming design. The optimization problem for the joint design of the digital beamforming at the BS and the analog reflective+refractive beamforming at the IOS is formulated in Section IV, and an iterative algorithm for solving the resulting non-convex problem is introduced in Section V. The theoretical analysis of the optimal phase shifts and the optimal power ratio that maximizes the sum-rate of the network are elaborated in Section VI. Numerical results are

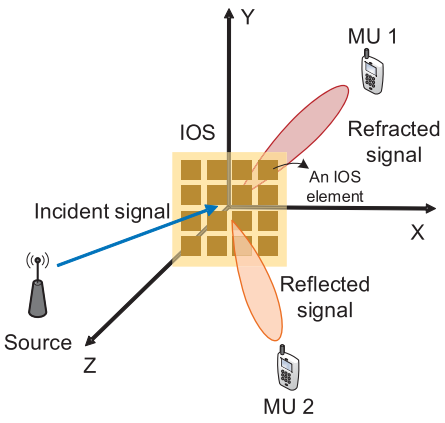

(a) Reflected and refracted signals from an IOS.

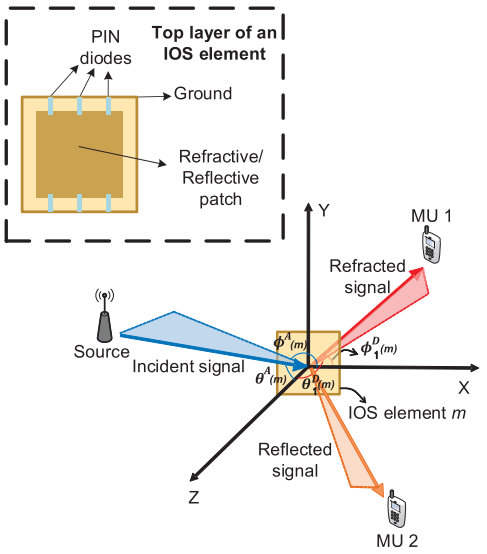

(b) Reflected and refracted signals for a single reconfigurable element of the IOS.

Fig. 1. Illustration of the reflected and refracted signals in an IOS-assisted communication system.

illustrated in Section VII in order to quantitatively evaluate the performance of the proposed algorithm. Finally, conclusions are drawn in Section VIII.

Notation: Boldface lower and upper case symbols denote vectors and matrices, respectively. Conjugate transpose and transpose operators are denoted by $(\cdot)^H$ and $(\cdot)^T$, respectively. $\mathrm{Tr}\{\cdot\}$ is the trace operator. $[\boldsymbol{A}]^{k,m}$ denotes the (k,m)th element of matrix $\boldsymbol{A}$, and $\boldsymbol{A}^i$ is the ith column of matrix $\boldsymbol{A}$.

II. Intelligent Omni-Surface

An IOS is a two-dimensional array of electrically controllable scattering elements, as illustrated in Fig. 1(a). In particular, the considered IOS is made of M reconfigurable elements of equal size. The size of each element is δ_x and δ_y along the x and y axis, respectively. Each reconfigurable element consists of multiple metallic patches and N_D PIN diodes that are evenly distributed on a dielectric substrate. The metallic patches are connected to the ground via the PIN diodes that can be switched between their ON and OFF states according to predetermined bias voltages. The ON/OFF configuration of the PIN diodes determines the phase response applied by the IOS to the incident signals. In total, each metallic patch can introduce 2^{N_D} different phase shifts to the incident signals. For generality, we assume that a subset of the possible phase shifts is available, which is referred to as the *available phase shift set* and is denoted by $\mathcal{S}_a = \{1, \ldots, S_a\}$. The phase shift of the mth reconfigurable element is denoted by $\psi_m \in \mathcal{S}_a$. The S_a available phase shifts are uniformly distributed with a discrete phase shift step equal to $\Delta\psi_m = \frac{2\pi}{S_a}$ [28]. Therefore, the possible values of the phase shifts are $l_m \Delta\psi_m$, where l_m is an integer satisfying $0 \leq l_m \Delta\psi_m \leq S_a - 1$. The vector of phase shifts of the M elements of the IOS is denoted by $\boldsymbol{s} = (\phi_1, \ldots, \phi_M)$. When a signal impinges, from either sides of the surface, upon one of the M reconfigurable elements of the IOS, a fraction of the incident power is reflected and refracted towards the same side and the opposite side of the impinging signal. This makes an IOS different from an IRS [38]. The phase shifts of the reflected and refracted signals can be either the same or different, which depends on the structure of the IOS elements [39]–[41]. In this paper, we consider the case where the reflected and refracted signals of an IOS share the same phase shift.

The direction of the signal that is emitted by the transmitter and that impinges upon the mth reconfigurable element of the IOS is denoted by $\xi^A(m) = (\theta^A(m), \phi^A(m))$, and the direction of the signal that is re-emitted by the mth reconfigurable element of the IOS towards the ith MU is denoted by $\xi_i^D(m) = (\theta_i^D(m), \phi_i^D(m))$, respectively, as illustrated in Fig. 1(b). The response of the mth reconfigurable element of the IOS to the incident signal is denoted by the complex coefficient g_m, which is referred to as the *amplitude gain* of the signal. In particular, g_m depends on the direction of incidence i.e., $\xi^A(m)$, the direction of departure (either in reflection or in refraction), i.e., $\xi_i^D(m)$, and the phase shift ψ_m. In mathematical terms, we have

$$g_m(\xi^A(m), \xi_i^D(m), \psi_m) = \sqrt{G_m K^A(m) K_i^D(m) \delta_x \delta_y |\gamma_m|^2} \exp(-j\psi_m), \quad (1)$$

where G_m is the antenna power gain of the mth reconfigurable element, and ψ_m is the corresponding phase shift. The coefficient $|\gamma_m|^2$ is the power ratio between the power of the signal re-emitted by the IOS and the power of the incident signal. Depending on the implementation of the IOS, $|\gamma_m|^2$ can be either a function of ψ_m or a constant. In this paper, for simplicity, we assume that $|\gamma_m|^2$ is independent of the phase shift ψ_m [20]. $K^A(m)$ and $K_i^D(m)$ are the normalized power radiation patterns of the incident and the re-emitted (either reflected or refracted) signal, respectively. An example for the normalized power radiation patterns is the following [42]

$$K^A(m) = |\cos^3 \theta^A(m)|, \quad \theta^A(m) \in (0, \pi), \quad (2)$$

$$K_i^D(m) = \begin{cases} \frac{1}{1+\epsilon} |\cos^3 \theta_i^D(m)|, & \theta_i^D(m) \in (0, \pi/2), \\ \frac{\epsilon}{1+\epsilon} |\cos^3 (\theta_i^D(m))|, & \theta_i^D(m) \in (\pi/2, \pi), \end{cases} \quad (3)$$

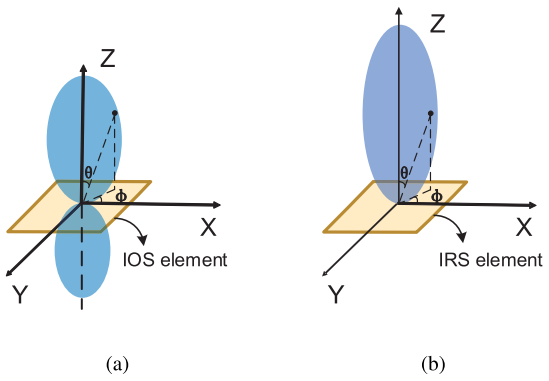

(a) (b)

Fig. 2. Normalized power radiation pattern of (a) an IOS element, (b) an IRS element.

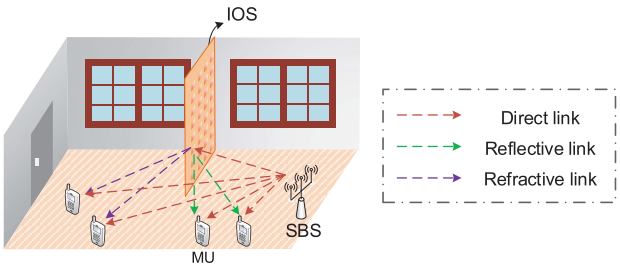

Fig. 3. System model for the IOS-aided downlink cellular system.

where ϵ is a constant parameter that quantifies the power ratio between the reflected and refracted signals of the IOS, which is determined by the structure and hardware implementation of the reconfigurable elements [43]. It is worth noting that the strength of both the reflected and refracted signals satisfy (3), where $\theta_i^D(m) \in (0, \pi/2)$ refers to the reflected signals, and $\theta_i^D(m) \in (\pi/2, \pi)$ refers to the refracted signals. The normalized power radiation pattern of an IOS element is illustrated in Fig. 2, and it is compared against the same normalized power radiation pattern of a conventional IRS. Since the IOS is intended to be a passive device with no active power sources, the sum of the refracted and reflected power cannot exceed the power of the incident signals. Therefore, the following property holds

$$\int_0^{2\pi} \int_0^{\pi} |g_m(\xi^A(m), \xi^D(m), \psi_m)|^2 d\theta d\phi \leq 1. \tag{4}$$

III. System Model

In this section, we first describe the considered IOS-assisted downlink system model where a multi-antenna BS serves multiple MUs, and we then introduce the transmission channel model of the IOS-assisted system. Finally, the joint BS and IOS beamforming design for the considered transmission system is described.

A. Scenario Description

As shown in Fig. 3, we consider a downlink transmission scenario in an indoor environment, which consists of one small BS (SBS) with K antennas and N single-antenna MUs that are denoted by $\mathcal{N} = \{1, 2, \ldots, N\}$. Due to the complex scattering characteristics in indoor environments, some MUs that are far from the SBS may undergo severe fading, which leads to a low QoS for the corresponding communication links. To tackle this problem, we deploy an IOS in the considered indoor environment in order to extend the service coverage and to enhance the strength of the signals received by the MUs. As mentioned, the IOS consists of M reconfigurable elements that are denoted by $\mathcal{M} = \{1, 2, \ldots, M\}$. The MUs are split into two subsets according to their locations with respect to the IOS. The set of MUs that receive the signals *reflected* from the IOS is denoted by $\mathcal{N}_r$, and the set of MUs that receive the signals *refracted* from the IOS is denoted by $\mathcal{N}_t$, with $\mathcal{N}_r \cap \mathcal{N}_t = \varnothing$, and $\mathcal{N}_r \cup \mathcal{N}_t = \mathcal{N}$. In this paper, the IOS can be viewed as an antenna array that is inherently capable of realizing analog beamforming by appropriately optimizing the phase shifts of the M reconfigurable elements of the IOS. This is elaborated in Section III-C.

B. Channel Model

The channel from the SBS to each MU consists of two parts: the reflected or refracted path that is induced by the IOS, and the direct path from the SBS to the MU.

1) Reflected-Refracted Channel via the IOS: As mentioned in Section II, the signal re-emitted by the IOS (see Fig. 1(a)) is given by the sum of two concurrent contributions: the refracted signal and the reflected signal. The location of each MU determines whether it receives the refracted signal or the reflected signal from the IOS. The channel from the SBS to the MU via the IOS is given by the sum of the M channels through the M reconfigurable elements of the IOS. Each of the M SBS-IOS-MU links is model as a Rician channel in order to take into account the LoS contribution and the non-LOS (NLoS) multipath components. In particular, the channel gain from the kth antenna of the SBS to the ith MU via the mth reconfigurable element of the IOS is given by

$$h_{i,k}^m = \sqrt{\frac{\kappa}{1+\kappa}} h_{i,k}^{m,LoS} + \sqrt{\frac{1}{1+\kappa}} h_{i,k}^{m,NLoS}. \tag{5}$$

The LoS component of $h_{i,k}^m$ is expressed as

$$h_{i,k}^{m,LoS} = \frac{\lambda \sqrt{G_k^{tx} K^A(m) G_i^{rx} K_i^D(m)} e^{\left(\frac{-j2\pi(d_{k,m}+d_{m,i})}{\lambda}\right)}}{(4\pi)^{\frac{3}{2}} d_{k,m}^{\alpha} d_{m,i}^{\alpha}} \times g_m(\xi_k^A(m), \xi_i^D(m), \psi_m), \tag{6}$$

where λ is the signal wavelength, G_k^{tx} and G_i^{rx} are the power gains of the kth antenna of the SBS and the antenna of the ith MU, respectively. $K^A(m)$ is the normalized power gain of the kth antenna of the SBS in the direction of the mth reconfigurable element of the IOS, and $K_i^D(m)$ is the normalized power gain of the ith MU in the direction of the mth reconfigurable element of the IOS, which are given in (2) and (3), respectively. $d_{k,m}$ and $d_{m,i}$ are the transmission distances between the mth reconfigurable element of the IOS and the kth antenna of the SBS and the ith MU, respectively, and α is the corresponding path-loss exponent. In addition, $g_m(\xi_k^A(m), \xi_i^D(m), \psi_m)$ is given and defined in (1).

The NLoS component of $h_{i,k}^{m}$ is expressed as

$$h_{i,k}^{m,NLoS} = PL(k,m,i)h^{SS}, \tag{7}$$

where $PL(k,m,i)$ is the path-loss of the SBS-IOS-MU link given in (6), and $h^{SS} \sim \mathcal{CN}(0,1)$ accounts for the cumulative effect of the large number of scattered paths that originate from the random scatterers available in the propagation environment.

2) BS-MU Direct Path: As far as the BS-MU channel is concerned, we assume a Rayleigh fading model. Therefore, the channel gain from the kth antenna of the SBS to the ith MU is

$$h_{i,k}^{D} = \sqrt{G_k^{tx} F_{k,i} G_i^{rx} d_{i,k}^{-\alpha}} h^{SS}, \quad \forall i \in \mathcal{N}, \tag{8}$$

where $F_{k,i} = |\cos^3 \theta_{k,i}^{tx}||\cos^3 \theta_{k,i}^{rx}|$ is the normalized end-to-end power gain of the kth antenna of the SBS and the ith MU, where $\theta_{k,i}^{tx}$ is the angle between the kth antenna of the SBS and the direction to the ith MU, and $\theta_{k,i}^{rx}$ is the angle between the antenna of the ith MU and the direction to the kth antenna of the SBS. $d_{i,k}$ is the distance between the kth antenna of the SBS and the ith MU.

In summary, the channel gain from the kth antenna of the SBS to the ith MU can be written as

$$h_{i,k} = \sum_{m=1}^{M} h_{i,k}^{m} + h_{i,k}^{D}, \quad \forall i \in \mathcal{N}, \tag{9}$$

where the first term represents the superposition of the reflected or refracted path of the M reconfigurable elements of the IOS, and the second term is the direct path.

C. IOS-Based Beamforming

In this section, we introduce the IOS-based beamforming design that allows the IOS to reflect and refract the incident signals towards specified locations of the MUs. Since the reconfigurable elements of the IOS have no digital processing capabilities, we consider a hybrid beamforming scheme, where the digital beamforming is performed at the SBS and the analog beamforming is performed at the IOS. Furthermore, due to practical implementation constraints, discrete phase shifts are assumed at the IOS. An example of the hybrid beamforming for $|\mathcal{N}_r| = 1$ and $|\mathcal{N}_t| = 1$ is shown in Fig. 4.

1) Digital Beamforming at the SBS: The SBS first encodes the N different data streams that are intended to the MUs via a digital beamformer, $\mathbf{V}_D$, of size $K \times N$, with $K \geq N$, and then emits the resulting signals through the K transmit antennas. We denote the intended signal vector for the N MUs by $\mathbf{x} = [x_1, x_2, \ldots, x_N]^T$. The transmitted vector of the SBS is given by

$$\mathbf{y} = \mathbf{V}_D \mathbf{x}. \tag{10}$$

We denote the maximum transmission power of the SBS by P_B, hence the power constraint for the digital beamformer can be expressed as

$$\mathrm{Tr}\left(\mathbf{V}_D \mathbf{V}_D^H\right) \leq P_B. \tag{11}$$

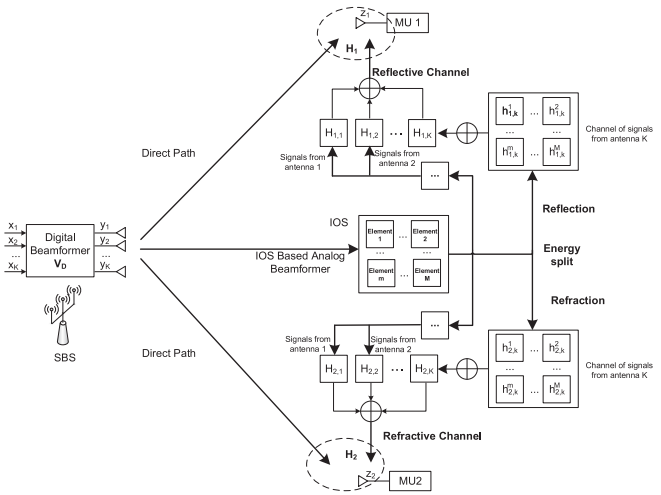

Fig. 4. Block diagram of the IOS-based beamforming for 2 MUs.

2) IOS-Based Analog Beamforming: The received signal at the ith MU can be expressed as

$$z_i = \sum_{k=1}^{K} h_{i,k} \mathbf{V}_D^{k,i} x_i + \sum_{i \neq i'} \sum_{k=1}^{K} h_{i,k} \mathbf{V}_D^{k,i'} x_{i'} + w_i, \tag{12}$$

where w_i is the additive white Gaussian noise (AWGN) at the ith MU whose mean is zero and whose variance is σ^2. Therefore, the N signals of the MUs in (12) can be cast in a vector $\mathbf{z} = [z_1, z_2, \ldots, z_N]^T$ as follows:

$$\mathbf{z} = \mathbf{H}\mathbf{V}_D \mathbf{x} + \mathbf{w}, \tag{13}$$

where $\mathbf{w} = [w_1, w_2, \ldots, w_N]^T$ is the noise vector, and $\mathbf{H} = \begin{bmatrix} h_{1,1} & \ldots & h_{1,K} \\ \ldots & \ldots & \ldots \\ h_{N,1} & \ldots & h_{1,K} \end{bmatrix}$ is the $N \times K$ compound channel matrix, which accounts of the propagation channel and for the phase shifts (analog beamforming) applied by the IOS (see (1) and (9)).

From (13), the downlink data rate of the ith MU can be formulated as

$$R_i = W_B \log_2 \left(1 + \frac{|(\mathbf{H}^i)^H \mathbf{V}_D^i|^2}{|\sum_{i \neq i'} (\mathbf{H}^i)^H \mathbf{V}_D^{i'}|^2 + \sigma^2}\right), \tag{14}$$

where W_B is the bandwidth, $\mathbf{H}^i$ and $\mathbf{V}_D^i$ are the ith column of matrices $\mathbf{H}$ and $\mathbf{V}_D$, respectively. It is worth noting that (14) is different from the rate in an IRS-assisted communication system, since the matrix $\mathbf{H}$ accounts for both the reflective and refractive channels.

IV. Problem Formulation and Decomposition

In this section, we first formulate a joint IOS phase shift design and SBS digital beamforming optimization problem to maximize the system sum-rate. Then, we decouple the resulting non-convex optimization problem into two subproblems.

A. Problem Formulation

As shown in (6) and (14), the achievable rate of an MU is determined by the phase shifts of the IOS $\boldsymbol{s}$ and by the digital

beamformer of the SBS $\mathbf{V}_D$. With an appropriate design of the IOS phase shifts and SBS digital beamformer, the signal-to-interference+noise ratio (SINR) at the MUs can be improved, and the data rate of the MUs can be enhanced. To study the impact of the IOS on the MUs in terms of both reflected and refracted signals, we aim to maximize the sum-rate of the N MUs in the system by jointly optimizing the IOS phase shifts $\boldsymbol{s}$ and the SBS digital beamformer $\mathbf{V}_D$. In particular, this optimization problem can be formulated as

$$\max_{\boldsymbol{s},\mathbf{V}_D} \sum_{i=1}^{N} R_i, \tag{15a}$$

$$s.t.\ \mathrm{Tr}\left(\mathbf{V}_D\mathbf{V}_D^H\right) \leq P_B, \tag{15b}$$

$$\psi_m \in \mathcal{S}_a, \quad m = 1, 2, \ldots, M. \tag{15c}$$

In (15), constraint (15b) accounts for the maximum power budget of the SBS, and constraint (15c) denotes the feasible set of the phase shift of each IOS reconfigurable element.

B. Problem Decomposition

Problem (15) is a mixed-integer non-convex optimization problem that consists of the discrete-valued variables $\boldsymbol{s}$ and the continuous-valued variables $\mathbf{V}_D$. Therefore, (15) is known to be a complex optimization problem to solve. To tackle it, we decouple (15) into two subproblems: (i) the optimization of the digital beamforming at the SBS and (ii) the optimization of the analog beamforming (phase shifts) at the IOS.

1) Digital Beamforming Optimization at the SBS: To optimize the digital beamforming at the SBS, we set the phase shifts of the IOS, i.e. $\boldsymbol{s}$, to fixed values. Therefore, (15) reduces to

$$\max_{\mathbf{V}_D} \sum_{i=1}^{N} R_i, \tag{16a}$$

$$s.t.\ \mathrm{Tr}\left(\mathbf{V}_D\mathbf{V}_D^H\right) \leq P_B. \tag{16b}$$

2) Analog Beamforming Optimization at the IOS: To optimize the phase shifts of the IOS, we assume that the digital beamforming matrix $\mathbf{V}_D$ is given. Therefore, (15) reduces to

$$\max_{\boldsymbol{s}} \sum_{i=1}^{N} R_i, \tag{17a}$$

$$s.t.\ \psi_m \in \mathcal{S}_a, \quad m = 1, 2, \ldots, M. \tag{17b}$$

V. Sum-Rate Maximization: Algorithm Design

In this section, we first design two algorithms to solve subproblems (16) and (17) individually, and we then devise an iterative algorithm for solving (15).

A. Digital Beamforming Optimization at the SBS

In this section, we solve the digital beamforming optimization at the SBS stated in (16). In particular, we consider zero-forcing (ZF) beamforming and optimal transmit power optimization, in order to alleviate the interference among the MUs. As introduced in [28], the ZF-based digital beamforming can be formulated as

$$\mathbf{V}_D = \mathbf{H}^H(\mathbf{H}\mathbf{H}^H)^{-1}\mathbf{P}^{1/2} = \widetilde{\mathbf{V}}_D\mathbf{P}^{1/2}, \tag{18}$$

where $\widetilde{\mathbf{V}}_D = \mathbf{H}^H(\mathbf{H}\mathbf{H}^H)^{-1}$ and $\mathbf{P}$ is a diagonal matrix whose ith diagonal element, which is denoted by p_i, is the received power at the ith MU.

Based on the ZF beamforming design in (18), problem (16) can be simplified as

$$\max_{p_i \geq 0} \sum_{i=1}^{N} W_B \log_2\left(1 + \frac{p_i}{\sigma^2}\right), \tag{19a}$$

$$s.t.\ \mathrm{Tr}\left(\mathbf{P}^{1/2}\widetilde{\mathbf{V}}_D^H\widetilde{\mathbf{V}}_D\mathbf{P}^{1/2}\right) \leq P_B. \tag{19b}$$

The optimal solution of problem (19) is the well-known water-filling power allocation [44]

$$p_i = \frac{1}{\nu_i}\max\left(\frac{1}{\mu} - \nu_i\sigma^2, 0\right), \tag{20}$$

where ν_i is the ith diagonal element of $\widetilde{\mathbf{V}}_D^H\widetilde{\mathbf{V}}_D$ and μ is a normalization factor that fulfills the constraint $\sum_{i=1}^{N}\max\left(\frac{1}{\mu} - \nu_i\sigma^2, 0\right) = P_B$. After obtaining $\mathbf{P}$ through the water-filling algorithm, the digital beamforming matrix is directly obtained from (18).

B. Analog Beamforming Optimization at the IOS

In this section, we solve the analog beamforming optimization at the IOS stated in (17). Since the digital beamforming is assumed to be fixed and to be given by the ZF-based precoding matrix in (19), the problem in (17) can be simplified as

$$\max_{\boldsymbol{s}} \sum_{i=1}^{N} W_B \log_2\left(1 + \frac{|(\mathbf{H}^i)^H\mathbf{V}_D^i|^2}{\sigma^2}\right), \tag{21a}$$

$$s.t.\ 0 \leq \psi_m < 2\pi, \quad m = 1, 2, \ldots, M. \tag{21b}$$

Problem (21) is tackled in two steps: (i) first, a relaxed problem that assumes continuous phase shifts is considered, and (ii) then, a branch-and-bound based algorithm is proposed to account for the discrete phase shifts.

1) Continuous IOS Phase Shift Design: According to the channel model introduced in Section III-B, the objective function in (21a) can be approximated to a concave function with respect to the phase shift of each reconfigurable element of the IOS. Therefore, problem (21) can be solved by optimizing the phase shifts of the M reconfigurable elements iteratively. More precisely, the downlink data rate of each MU, i.e., R_i, can be approximated to a concave function of each variable in $\boldsymbol{s}$. Therefore, the objective function in (21a), i.e., $\sum_{i=1}^{N} R_i$, is approximately a concave function of each variable in $\boldsymbol{s}$ while keeping the others fixed. To optimize the phase shifts of all the reconfigurable elements of the IOS, we first set a random initial solution, which is denoted by $\boldsymbol{s}^0 = (s_1^0, \ldots, s_M^0)$. Then, we iteratively optimize the phase shift of each reconfigurable element. Without loss of generality, let us consider the optimization of ψ_m at the rth iteration. We fix the phase shift of all the other reconfigurable elements at the newly solved value,

Algorithm 1: Continuous IOS Phase Shift Design

1: **Initialization:** Set an initial solution $\boldsymbol{s}^0 = (s_1^0, \ldots, s_M^0)$ to problem (21)
2: **While** $\sum_{m=1}^{M} \Delta R_m^r \geq R_{th}$
3: **For** $m = 1 : M$
4: Solve ψ_m in problem (21) while keeping the other variables fixed
5: Compute ΔR_m^r in (22)
6: Update the IOS phase shifts to $\boldsymbol{s} = (s_1 = s_i^r, \ldots, s_m = s_m^r, s_{m+1} = s_{m+1}^{r-1}, \ldots s_M = s_M^{r-1})$
7: **Output:** $\boldsymbol{s}$

i.e., $s_1 = s_1^r, \ldots, s_{m-1} = s_{m-1}^r, s_{m+1} = s_{m+1}^{r-1}, \ldots, s_M = s_M^{r-1}$, and maximize $\sum_{i=1}^{N} W_B \log_2 \left(1 + \frac{|(\mathbf{H}^i)^H \mathbf{V}_D^i|^2}{\sigma^2}\right)$ as a function of only ψ_m as mentioned above. The obtained solution ψ_m^r is then updated as a temporary solution for the phase shift of the mth reconfigurable element, and the corresponding sum-rate increment is given by

$$\Delta R_m^r = \sum_{i=1}^{N} \log_2 \left(1 + \frac{|(\mathbf{H}^i)^H \mathbf{V}_D^i|^2}{\sigma^2}\right)|_{s_m^r}, - \sum_{i=1}^{N} \log_2 \left(1 + \frac{|(\mathbf{H}^i)^H \mathbf{V}_D^i|^2}{\sigma^2}\right)|_{s_m^{r-1}}. \quad (22)$$

The algorithm terminates when the increment of the downlink sum-rate between two consecutive iterations is below a specified threshold, i.e., $\sum_{m=1}^{M} \Delta R_m^r < R_{th}$. Since problem (21) is not jointly convex with respect to all the variables in $\boldsymbol{s}$, the proposed solution converges to a locally optimal solution. The convergence of the proposed algorithm is analyzed in Section V-C. The proposed continuous IOS phase shift design is summarized in Algorithm 1.

2) Discrete IOS Phase Shift Design: By applying Algorithm 1, the continuous phase shifts of the M reconfigurable elements are obtained, which are denoted by ψ_m^{opt}, $m = 1, 2, \ldots, M$. However, ψ_m^{opt} may not correspond to any of the finite and discrete phase shifts in $\mathcal{S}_a$. In general, in fact, the continuous phase shift of the mth reconfigurable element of the IOS that is solution of problem (21) lies in the range determined by the two consecutive phase shifts $l_m \Delta\phi_m$ and $(l_m + 1)\Delta\phi_m$, i.e., $l_m \Delta\phi_m \leq \psi_m^{opt} \leq (l_m + 1)\Delta\phi_m$. Therefore, after computing the continuous phase shifts of the IOS with the aid of Algorithm 1, the search space for the M discrete phase shifts still encompasses 2^M possibilities. To overcome the associated computational complexity, we propose an efficient branch-and-bound algorithm that yields the optimal discrete phase shifts of the IOS that belong to the finite set $\mathcal{S}_a$.

The solution space of the IOS phase shift vector $\boldsymbol{s}$ can be viewed as a binary tree structure, as shown in Fig. 5. Each node of the tree contains the phase shift information of all the M reconfigurable elements, i.e., $\boldsymbol{s} = (s_1, \ldots, s_M)$. At the root node, all the variables in $\boldsymbol{s}$ are unfixed. After applying Algorithm 1, the value of an unfixed variable ψ_m at a father node can be one of the two phase shifts $l_m \Delta\phi_m$ or $(l_m + 1)\Delta\phi_m$. As illustrated in Fig. 5, this branches the father node into two child nodes. This operation can be repeated for each parent node. Our objective is to devise an efficient algorithm that allows us to solve problem (17) based on the tree structure illustrated in Fig. 5, which is determined by Algorithm 1.

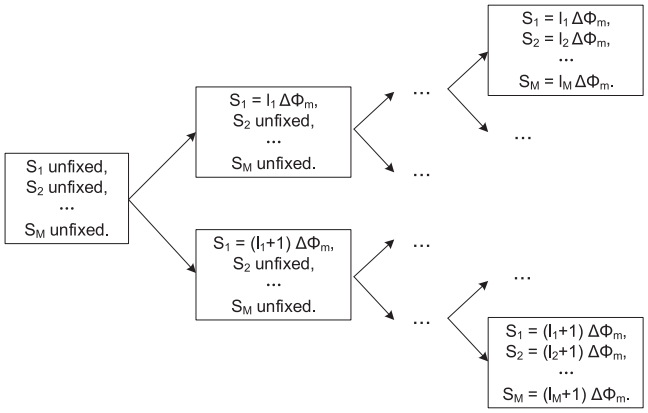

Fig. 5. Tree structure of the proposed branch-and-bound algorithm.

The proposed algorithm starts by randomly setting a feasible solution for the phase shift ψ_m to any of the two possible solutions $l_m \Delta\phi_m$ or $(l_m + 1)\Delta\phi_m$. The corresponding value of the objective function yields a lower bound to problem (21). Then, the proposed branch-and-bound algorithm recursively splits the search space of problem (17) into smaller search spaces based on the tree structure illustrated in Fig. 5. The search starts from the root node of the tree in a depth-first-search method. At each node, one of the unfixed variable is fixed, which branches the node into two child nodes. An upper bound for the sum-rate of each of the two child nodes is obtained solving problem (21) by relaxing the unfixed discrete variables $\mathbf{s}^{\mathbf{uf}}$ into continuous variables. The obtained upper bound for the rate is compared with the current lower bound, and, depending on their relation, the branch that corresponds to the node under analysis is either kept or pruned. The lower bound is compared to the sum-rate of a node if all its variables are fixed, and is updated to the larger one between the two values. The process is iterated until all the nodes of the tree in Fig. 5 are either visited or pruned. The details of the branch-and-bound method that solves the IOS phase shift design problem (17) is summarized in Algorithm 2.

C. Joint SBS Digital Beamforming and IOS Phase Shift Optimization

Based on the proposed solutions for the ZF-based digital beamforming at the SBS and the branch-and-bound algorithm for obtaining the discrete phase shifts of the IOS by leveraging Algorithm 1 and Algorithm 2, problem (15) can be solved by using alternating optimization as summarized in Algorithm 3. Given the phase shifts of the reconfigurable elements, the analog beamforming can be considered as part of the channel vector, and the ZF precoding of the SBS digital beamforming can be designed accordingly to eliminate the interference [45]. When the phase shifts of the reconfigurable elements are

Algorithm 2: IOS Phase Shift Design

1: **Initialization:** Set an initial feasible solution $\boldsymbol{s}$ to problem (17) based on Algorithm 1 and set the corresponding sum-rate R_{lb} as the lower bound
2: **While** All nodes in Fig. 5 are not visited or pruned
3: Calculate the upper bound of the current node $R_{ub} = \max_{\boldsymbol{s}^{uf}} \sum_{i=1}^{N} \log_2\left(1 + \frac{|(\mathbf{H}^i)^H \mathbf{V}_D^i|^2}{\sigma^2}\right)$
4: **If** $R_{ub} < R_{lb}$: Prune the corresponding branch; Return
5: **Else**:
6: **If** The current node has any child nodes that is not pruned: Move to one of its two child nodes; Continue
7: **Else** Calculate the corresponding sum-rate R_{curr}
8: **If** $R_{curr} > R_{lb}$: $R_{lb} = R_{curr}$; Return
9: **Output:** $\boldsymbol{s}$

Algorithm 3: Joint SBS Digital Beamforming and IOS Phase Shift Optimization

1: **While** The sum-rate difference between two consecutive iterations is below a threshold ω
2: Perform SBS digital beamforming as introduced in Section V-A
3: Compute the continuous IOS phase shifts by leveraging Algorithm 1
4: Compute the discrete IOS phase shifts by leveraging Algorithm 2
5: Update the ZF precoding of the SBS digital beamforming
6: Obtain the maximum sum-rate of the IOS-assisted communication system

changed, the ZF precoding needs to be adjusted correspondingly. The convergence and complexity of Algorithm 3 are analyzed in the following two propositions.

Proposition 1: The proposed joint SBS digital beamforming and IOS analog beamforming optimization algorithm is convergent to a locally optimum solution.

Proof: We denote the sum-rate at the rth iteration by $\mathcal{R}(\boldsymbol{s}^r, \mathbf{V}_D^r)$. At the $(r+1)$th iteration, the solution of the optimal SBS digital beamforming given by $\boldsymbol{s} = \boldsymbol{s}^r$ yields a sum-rate $\mathcal{R}(\boldsymbol{s}^r, \mathbf{V}_D^{r+1}) \geq \mathcal{R}(\boldsymbol{s}^r, \mathbf{V}_D^r)$. Similarly, the solution of the optimal IOS analog beamforming given by $\mathbf{V}_D = \mathbf{V}_D^{r+1}$ yields a sum-rate $\mathcal{R}(\boldsymbol{s}^{r+1}, \mathbf{V}_D^{r+1}) \geq \mathcal{R}(\boldsymbol{s}^r, \mathbf{V}_D^{r+1})$. Therefore, we obtain the following inequalities $\mathcal{R}(\boldsymbol{s}^{r+1}, \mathbf{V}_D^{r+1}) \geq \mathcal{R}(\boldsymbol{s}^r, \mathbf{V}_D^{r+1}) \geq \mathcal{R}(\boldsymbol{s}^r, \mathbf{V}_D^r)$, i.e., the sum-rate does not decrease at each iteration of Algorithm 3. Since the sum-rate is upper bounded thanks to the constraint on the total transmit power, Algorithm 3 converges in a finite number of iterations to a locally optimum solution. □

Proposition 2: The complexity of each iteration of the proposed joint SBS digital beamforming and IOS analog beamforming optimization algorithm is $O(2^M + N)$.

Proof: At each iteration, the SBS digital beamforming problem for the N MUs can be solved by using convex optimization methods. As mentioned in [46], the complexity of convex optimization can be $O(N)$. The complexity of the IOS analog beamforming problem is the sum of the complexities of Algorithm 1 and Algorithm 2. Algorithm 1 is also based on convex optimization, with the complexity being $O(N)$, and the complexity of the branch-and-bound based Algorithm 2 is, in the worst case, $O(2^M)$. Therefore, the complexity of each iteration of Algorithm 3 is $O(N) + O(N) + O(2^M) = O(2^M + N)$. □

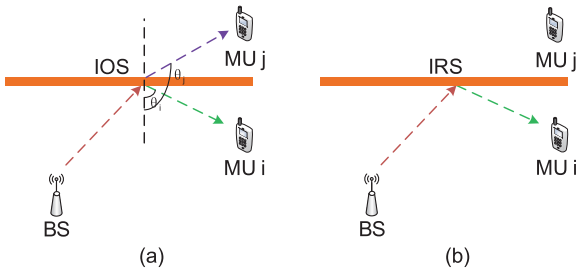

Fig. 6. Examples of MU distributions for the performance analysis of an IOS-assisted communication system. (a) IOS setup in which two MUs are located symmetrically with respect to the IOS; (b) IRS setup in which only reflections are allowed.

VI. Performance Analysis of the IOS-Assisted Communication System

In this section, we first discuss the impact of the phase shift design on the reflected and refracted signals, and we then analyze the downlink sum-rate as a function of the power ratio of the reflected and refracted signals. For ease of understanding, the impact of small-scale fading is ignored, and only the impact of the distances, the radiation pattern of the reconfigurable elements of the IOS, and the power allocation ratio between the reflected and refracted signals are considered.

A. Analysis of the Phase Shift Design

Our objective is to study the relation between the optimal phase shifts of the IOS when it is used as a refractive and reflective surface, and to understand the differences between these two cases. For analytical convenience, we assume that the power ratio $|\gamma_m|^2$ between the power of the signal re-emitted by the IOS and the power of the incident signal is a constant value.

In order to understand the differences and similarities between an IRS (only reflections are allowed) and an IOS (both reflections and refractions are allowed simultaneously), the following proposition considers the case study with two MUs, when one MU (the ith MU) lies in the reflective side of the IOS and the other MU (the jth MU) lies in the refractive side of the IOS.

Proposition 3: Consider an IOS-assisted communication system with two MUs, which are denoted by the indices i and j. If the two users are located symmetrically with respect to the IOS, as shown in Fig. 6(a), and the impact of small-scale fading is ignored, the optimal SBS digital beamforming and IOS analog beamforming are the same for both MUs.

Proof: See Appendix A. □

In an IOS-assisted communication system, the IOS phase shifts are jointly designed for the MUs on both sides of the surface. The optimal IOS phase shift design for the MUs on both sides of the surface may be different from the design that only consider accounts for the MUs in $\mathcal{N}_r$ (i.e., in the reflective side of the surface) or in $\mathcal{N}_t$ (i.e., in the refractive side of the surface). Proposition 3, in particular, can be regarded as a special case in which the optimal solution can be guaranteed for two users, each of them located on one side of the IOS. To maximize the downlink sum-rate for multiple MUs located on both sides of the IOS, we introduce a priority-based approach that gives higher priority to either the MUs on the reflective or refractive sides of the IOS. In particular, the *priority index* of the ith MU, which describes the strength of the reflective/refractive channel gain with respect to its location, is defined as

$$\mathcal{P}_i = \begin{cases} \sum_{m=1}^{M} \frac{|\cos^3 \theta_i^D(m)|}{(1+\epsilon) d_{m,i}^{\alpha}}, & i \in \mathcal{N}_r, \\ \sum_{m=1}^{M} \frac{\epsilon |\cos^3 \theta_i^D(m)|}{(1+\epsilon) d_{m,i}^{\alpha}}, & i \in \mathcal{N}_t \end{cases} \tag{23}$$

Proposition 4: Let us assume that the distance between the SBS and the IOS is fixed and only the distances of the MUs change, as well as that the small-scale fading is not considered. Thanks to the IOS, the MU with the highest priority index in (23) obtains the largest data rate gain.

Proof: See Appendix B. □

Based on Proposition 4, the following remarks for some asymptotic regimes of the IOS-assisted communication system can be made.

Remark 1: When $\epsilon \to 0$, the IOS boils down to an IRS, and $\sum_{i\in\mathcal{N}_r} \mathcal{P}_i \gg \sum_{i\in\mathcal{N}_t} \mathcal{P}_i$ is satisfied. The IOS phase shift design only considers the MUs that belong to the set $\mathcal{N}_r$.

Remark 2: When $\epsilon \to \infty$, the IOS only refracts the signals towards the opposite side of the SBS, and $\sum_{i\in\mathcal{N}_r} \mathcal{P}_i \ll \sum_{i\in\mathcal{N}_t} \mathcal{P}_i$ is satisfied. The IOS phase shift design only considers the MUs that belong to the set $\mathcal{N}_t$.

B. Analysis of the Refraction/Reflection Power Ratio

In this section, we analyze the impact of the power ratio of the reflected and refracted signals ϵ on the sum-rate of an IOS-assisted communication system.

Proposition 5: Given the average distance between the IOS and the MUs, the power ratio of the reflected and refracted signals ϵ is positively correlated with the ratio of the number of MUs on the two sides of the IOS, i.e., $\epsilon \propto \mathcal{N}_t/\mathcal{N}_r$.

Proof: See Appendix C. □

Proposition 6: Given a pair of symmetrically located MUs as illustrated in Fig. 6(a), a larger proportion of the available power is allocated to the MUs with a weak direct link (i.e., low received power). More specifically, $\epsilon > 1$ when the sum of the received power of the direct links from the SBS to the MUs in $\mathcal{N}_r$ is larger than that of the MUs in $\mathcal{N}_t$. Otherwise, $\epsilon < 1$ holds.

Proof: See Appendix D. □

In particular, when the distance from the SBS to the IOS is much larger than the distance from the IOS to the MUs, the distance from the SBS to each MU is approximately the same. Therefore, (32) in Appendix C can be simplified as

$$\frac{d(R_i + R_j)}{d\epsilon} \simeq \frac{1}{\ln 2} \frac{\beta_i^2 (1-\epsilon)(1+\epsilon)}{(\epsilon\beta_i(1+\epsilon) + (1+\epsilon)^2)(\beta_i(1+\epsilon) + (1+\epsilon)^2)}. \tag{24}$$

From (24), we evince that the maximum value of $\sum_{i\in\mathcal{N}} \Delta R_i$ is obtained for $\epsilon = 1$. Therefore, the following remark follows.

Remark 3: When the distance from the SBS to the IOS is much larger than the distance from the IOS to the MUs, the IOS maximizes the throughput of the system for $\epsilon = 1$, i.e., the power of the refracted and reflected signals is the same.

The assumptions in Proposition 6 and Remark 3 are usually satisfied when the IOS is deployed at the cell edge for coverage extension. Therefore, an IOS with $\epsilon = 1$ is capable of maximizing the sum-rate of the MUs at the cell edge of an IOS-assisted communication system. Finally, the following proposition yields the largest theoretical gain that an IOS-assisted system provides with respect to the benchmark IRS-assisted system.

Proposition 7: The ratio of the downlink sum-rate of an IOS-assisted system and an IRS-assisted system is upper-bounded by two.

Proof: See Appendix E. □

Proposition 7 unveils that an IOS may double the downlink sum-rate when compared to an IRS. This upper-bound is, however, difficult to be attained because it requires that the signal-to-interference-plus-noise ratio is infinite, as discussed in Appendix E.

VII. Simulation Results

In this section, we evaluate the performance of the considered IOS-assisted system based on the proposed algorithm, and compare it with an IRS-assisted system [47] and a conventional cellular system in the absence of IRS or IOS. In the IRS-assisted system, the IRS only reflects the signals from the SBS to the MUs, and the surface does not work in refraction mode. In the conventional cellular system, the MUs receive only the direct links from the SBS without the assistance of a reconfigurable surface.

In the simulations, we set the height of the SBS and the center of the IOS at 2 m, and the distance between the SBS and the IOS is 100 m. The MUs are randomly deployed within a disk of radius 50 m centered at the IOS. The maximum transmit power of the SBS is $P_B = 40$ dBm, the carrier frequency is 5.9 GHz, the noise power is -96 dBm, the antenna separation at the SBS is 0.2 m, and the inter-distance between the reconfigurable elements of the IOS is 0.025 m (i.e., half of the wavelength). The numbers of MUs (N) and SBS antennas (K) are 5, and the power ratio of the reflected and refracted signals is $\epsilon = 1$ (unless stated otherwise). The path-loss exponent of the direct link is 3, and the Rician factor is $\kappa = 4$.

Fig. 7(a) illustrates the average sum-rate of the MUs as a function of the size of the IOS. The average sum-rate is defined as the average of the sum-rate in (15a) as a function of the spatial distribution of the MUs. The IOS is modeled as a

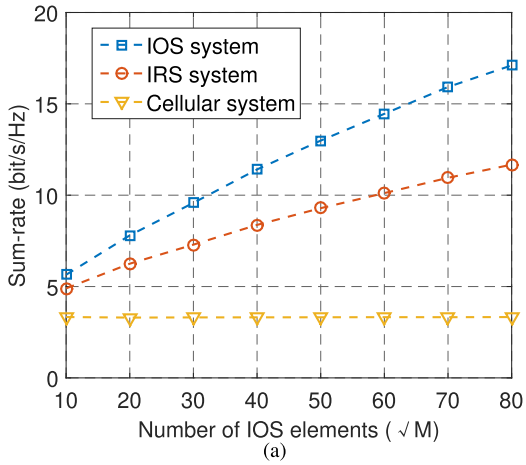

(a)

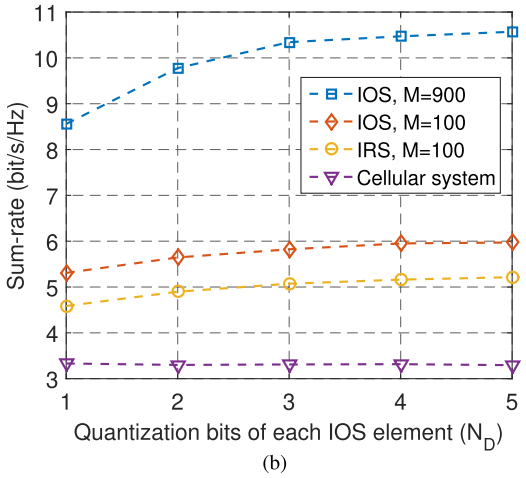

(b)

Fig. 7. Impact of the surface size and quantization bits on the sum-rate. (a) Number of IOS reconfigurable elements ($\sqrt{M}$) vs. sum-rate ($S_a = 4$); (b) Quantization bits of each IOS element (N_D) vs. sum-rate.

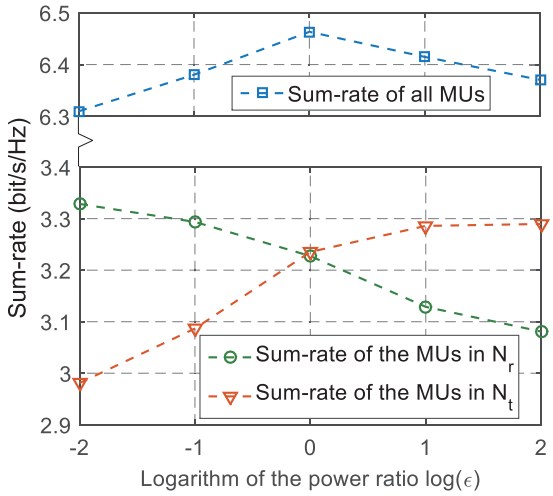

(a)

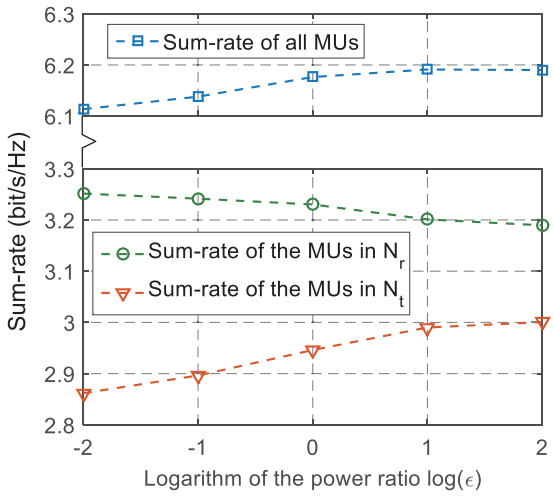

(b)

Fig. 8. Power ratio of the reflected and refracted signals (ϵ) vs. the sum-rate. (a) MU distribution radius: 2 m; (b) MU distribution radius: 20 m.

square array with $\sqrt{M}$ elements on each column and each row. The average sum-rate increases with the number of IOS reconfigurable elements, and the growth rate gradually decreases with the IOS size. An IOS with 30×30 elements improves the average sum-rate of about 2.9 times when compared to a conventional cellular system. On the other hand, an IRS of the same size improves the average sum-rate of about 2.3 times only. The IOS provides a higher average sum-rate since it is capable of providing service to the MUs that are located on both sides of the surface. The rate improvement offered by an IOS over an IRS is less than two, which is in agreement with Proposition 7.

Fig. 7(b) shows the average sum-rate as a function of the number of quantization bits N_D of each reconfigurable element of the IOS, with $N_D = \log_2(S_a)$. The average sum-rate increases with N_D and converges to a stable value as N_D increases. We observe, in particular, that few quantization bits are sufficient to achieve most of the average sum-rate and that the convergence rate increases with the size M of the IOS.

In Fig. 8, we analyze the relation between the average sum-rate and the power ratio of the reflected and refracted signals ϵ. In Fig. 8(a), the MUs are distributed around the IOS within a radius of 2 m, and the distance from the IOS to the MUs is much shorter than the distance from the SBS to the

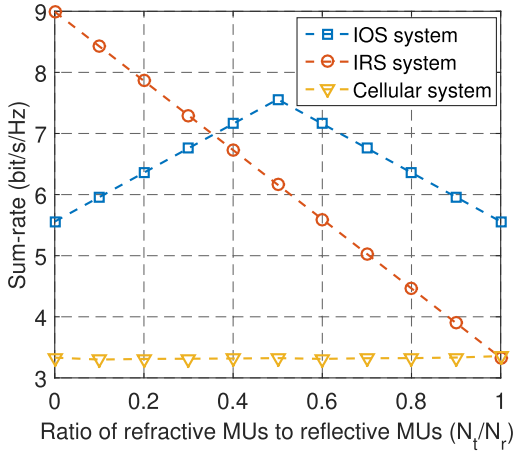

Fig. 9. Ratio of MUs receiving refracted signals to all MUs (N_t/N) vs. sum-rate.

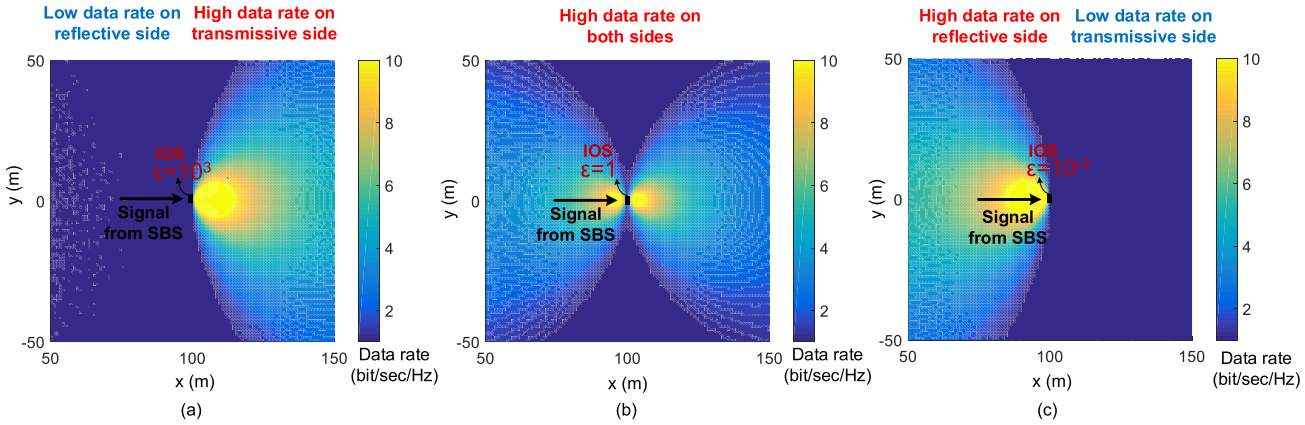

Fig. 10. Simulation of the maximum data rate with different ϵ. (a) $\epsilon = 10^3$. (b) $\epsilon = 1$. (c) $\epsilon = 10^{-3}$.

MUs. The average sum-rate of all the MUs is maximized for $\epsilon = 1$, which is in agreement with Remark 3. In Fig. 8(b), the MUs are distributed around the IOS within a radius of 20 m. In this configuration, the MUs in $\mathcal{N}_r$ receive a higher power through the direct links when compared to the MUs in $\mathcal{N}_t$. The average sum-rate is maximized if $\epsilon > 1$, which agrees with Proposition 6.

The impact of the distribution of the MU with respect to the location of the IOS is illustrated in Fig. 9. In the IOS-assisted communication system, the average sum-rate is maximized, in the considered setup, when the MUs are equally distributed on the two sides of the IOS (i.e., $N_r/N = 0.5$ in the figure). When the MUs are mostly located on one side of the IOS, i.e., $N_t/N \to 0$ or $N_t/N \to 1$, the power of the signals re-emitted by the IOS on both sides of the surface cannot be optimized for all the MUs concurrently. In an IRS-assisted communication system, on the other hand, the average sum-rate decreases linearly as a function of N_t/N, since an RIS can assist the transmission of only the MUs in $\mathcal{N}_r$.

In Fig. 10, we present the maximum sum-rate of a single MU at different locations, when the SBS is located on the left side of the surface. An IOS/IRS with 20×20 elements is deployed vertically with respect to the SBS at the location (100, 0), and the SBS is deployed at (0,0). Three different values for the power ratio of the reflected and refracted signals ϵ are illustrated.

If $\epsilon = 1$, the maximum sum-rate on both sides of the surface can be improved significantly. An omni-service extension is provided since the IOS is capable of enhancing the received power of the MUs on both sides of the surface. The MU can obtain a higher data rate when it is closer to the center of the IOS, where the reflective-refractive channel has a better quality. If $\epsilon = 10^3$ and $\epsilon = 10^{-3}$, most of the power is re-emitted to the right-hand and left-hand side of the IOS, respectively. This is in agreement with Remark 1 and Remark 2.

VIII. Conclusion

In this paper, we have introduced the IOS, which is a reconfigurable surface capable of concurrently reflecting and refracting impinging signals towards both sides of the surface. We have studied the utilization of the IOS in a multi-user downlink communication system. The IOS is capable of enhancing the received signals of the MUs on both sides of the surface through an appropriate design of the IOS phase shifts. We have formulated a joint IOS analog beamforming and SBS digital beamforming optimization problem to maximize the sum-rate of the system, and have proposed an iterative algorithm for efficiently solving it. From the obtained numerical simulations and analysis, three main conclusions can be drawn:

1) The sum-rate of an IOS-assisted communication system is higher than that of an IRS-assisted communication system. An IOS enhances the data rate of MUs located on both sides of the surface, which asymptotically double the achievable sum-rate and the service coverage.
2) The optimal power ratio of the reflected and refracted signals of the IOS is positively correlated with the ratio of the number of MUs on the two sides of the IOS, and is negatively correlated with the received power on the direct links from the SBS to the MUs.
3) The sum-rate of an IOS-assisted communication system increases with the geometric size of the surface and with the number of quantization bits of the phase shifts, but converges to a stable value when the IOS size and the quantization bits are sufficiently large.

Appendix A
Proof of Proposition 3

For a pair of MUs that are located symmetrically with respect to the IOS (e.g., the ith and jth MUs in Fig. 6(a)), the distance from each reconfigurable element to the two MUs is the same, i.e.,

$$d_{m,i} = d_{m,j}, \quad \forall m \in \mathcal{M}. \tag{25}$$

According to (3), the power radiation pattern of the reflected signals $K^D(m)|_r$ and that of the refracted signals $K^D(m)|_t$ of the MUs that are located symmetrically with respect to the

IOS satisfies the relation

$$\frac{K^D(m)|_r}{K^D(m)|_t} = \epsilon. \tag{26}$$

As shown in Fig. 6(a), in addition, the angles with respect to the normal to the surface satisfy the relation $\theta_i^D(m) + \theta_j^D(m) = \pi$, and then we have

$$|\cos(\theta_i^D(m))| = |\cos(\theta_j^D(m))|. \tag{27}$$

When substituting (25), (26), and (27) into (1), we have $\frac{g_m(\xi^A(m),\xi_j^D(m),\psi_m)}{g_m(\xi^A(m),\xi_i^D(m),\psi_m)} = \epsilon$ for any IOS phase shifts $\boldsymbol{s}$. If we assume that the antenna gains of the MUs are the same, and substitute (1) into (6), we have $\frac{h_{j,k}^{m,LoS}}{h_{i,k}^{m,LoS}} = \epsilon,\ \forall m \in \mathcal{M}, k \in \mathcal{K}$, and for any IOS phase shifts $\boldsymbol{s}$. Under these assumptions, and if the small-scale fading is not considered, we evince that the optimal SBS digital beamforming and IOS analog beamforming of the ith and jth MUs coincide. This concludes the proof.

Appendix B
Proof of Proposition 4

The improvement of data rate in the presence of an IOS is determined by the sum of the channel gains of the M SBS-IOS-MU links. Let us assume that the small scale fading can be ignored (long-term performance). From (1) and (6), the LoS component of the SBS-IOS-MU link from the kth antenna of the SBS to the ith MU via the mth reconfigurable element of the IOS is

$$h_{i,k}^{m,LoS} = \lambda K^A(m) K_i^D(m) \sqrt{G_k^{tx} G_m G_i^{rx} \delta_x \delta_y |\gamma_m|^2} \times \frac{\exp\left(\frac{-j2\pi(d_{k,m}+d_{m,i})}{\lambda} - j\psi_m\right)}{(4\pi)^{\frac{3}{2}} d_{k,m}^{\alpha} d_{m,i}^{\alpha}}, \tag{28}$$

The hardware-related parameters G_k^{tx}, G_m, G_i^{rx}, δ_x, δ_y, and γ_m can be considered as constants in a given IOS-assisted communication system. The phase shift of the SBS-IOS-MU link $\frac{-j2\pi(d_{k,m}+d_{m,i})}{\lambda} - j\psi_m$ is optimized with the algorithm proposed in Section V-B. Assuming that the locations of the SBS and IOS are given, the MU-related term that affects the channel gain of the LoS component is $\frac{K_i^D(m)}{d_{m,i}^{\alpha}},\ \forall i \in \mathcal{N}$, $k \in \mathcal{K}, m \in \mathcal{M}$. Therefore, the impact of the M reconfigurable elements can be expressed as

$$\mathcal{P}_i = \sum_{m=1}^{M} \frac{K_i^D(m)}{d_{m,i}^{\alpha}} = \begin{cases} \sum_{m=1}^{M} \frac{|\cos^3\theta_i^D(m)|}{(1+\epsilon) d_{m,i}^{\alpha}}, & i \in \mathcal{N}_r, \\ \sum_{m=1}^{M} \frac{\epsilon |\cos^3\theta_i^D(m)|}{(1+\epsilon) d_{m,i}^{\alpha}}, & i \in \mathcal{N}_t. \end{cases} \tag{29}$$

This concludes the proof.

Appendix C
Proof of Proposition 5

Assume that the signal-to-noise ratio (SNR) of the direct link from the SBS to the ith MU is α_i and that the SNR of the link from the IOS to the ith MU is β_i. The rate of the ith MU is

$$R_i = \log_2(1 + \alpha_i + \beta_i)^1. \tag{30}$$

Therefore, the sum-rate of all the MUs in the set $\mathcal{N}$ is given by $\sum_{k\in\mathcal{N}_r} R_k + \sum_{j\in\mathcal{N}_r} R_j$. Given the total power of the refracted and reflected signals, we aim to maximize the normalized sum-rate of the MUs, which is given as

$$\sum_{i\in\mathcal{N}} R_i = \sum_{k\in\mathcal{N}_r} \log_2(1 + \alpha_k + \frac{1}{1+\epsilon}\beta_k) + \sum_{j\in\mathcal{N}_t} \log_2(1 + \alpha_j + \frac{\epsilon}{1+\epsilon}\beta_j). \tag{31}$$

The first-order derivative of (31) with respect to ϵ is

$$\sum_{i\in\mathcal{N}} \frac{dR_i}{d\epsilon} = \frac{1}{\ln 2}\left(\sum_{j\in\mathcal{N}_t} \frac{\beta_j/(1+\epsilon)^2}{1 + \alpha_j + \frac{\beta_j \epsilon}{1+\epsilon}} - \sum_{k\in\mathcal{N}_r} \frac{\beta_k/(1+\epsilon)^2}{1 + \alpha_k + \frac{\beta_k}{1+\epsilon}}\right). \tag{32}$$

We denote the optimal value of ϵ that maximizes (31) by ϵ^{opt}. When the sum-rate is maximized, we have $\sum_{i\in\mathcal{N}} \frac{d\Delta R_i}{d\epsilon}|_{\epsilon=\epsilon^{opt}} = 0$.

If the MU j' is added to the set $\mathcal{N}_t$, a positive value is added to (32), and we have $\sum_{i\in\mathcal{N}} \frac{d\Delta R_i}{d\epsilon}|_{\epsilon=\epsilon^{opt}} > 0$. Thus, the sum-rate can be further improved by increasing ϵ. On the contrary, if the MU k' is added to the set $\mathcal{N}_r$, a negative value is added to (32). In this case a smaller value of ϵ improves the sum-rate of the system. This concludes the proof.

Appendix D
Proof of Proposition 6

We denote a pair of symmetrically-located MUs that receive the reflected signals and refracted signals by MU i and MU j, respectively, as shown in Fig. 6(a). Based on the notation and formulas introduced in Appendix C, the normalized sum-rate of the MUs can be given as ($\beta_j = \beta_i$ since the MUs are located symmetrically with respect to the IOS)

$$R_i + R_j = \log_2\left(1 + \alpha_i + \frac{1}{1+\epsilon}\beta_i\right) + \log_2\left(1 + \alpha_j + \frac{\epsilon}{1+\epsilon}\beta_i\right). \tag{33}$$

The derivative function of (33) with respect to ϵ is

$$\frac{d(R_i + R_j)}{d\epsilon} = \frac{1}{\ln 2} \frac{\beta_i^2(1-\epsilon)(1+\epsilon) + \beta_i(1+\epsilon)^2(\alpha_i - \alpha_j)}{(\epsilon\beta_i(1+\epsilon) + (1+\epsilon)^2)(\beta_i(1+\epsilon) + (1+\epsilon)^2)}. \tag{34}$$

The optimal value of the power ratio of the reflected and refracted signals satisfies $\epsilon = \frac{\beta_i + \alpha_i - \alpha_j}{\beta_i - \alpha_i + \alpha_j}$. When $\alpha_i > \alpha_j$, we have $\epsilon > 1$. Otherwise, we have $\epsilon < 1$. This concludes the proof.

[1]For simplicity, we do not consider the specific impact of the phase shift optimization, and assume that the SNRs of the SBS-to-MU link and the IOS-to-MU link can just be added directly.

APPENDIX E
PROOF OF PROPOSITION 7

Consider the two case studies illustrated in Fig. 6. In the IRS-assisted communication system, the total power that impinges upon the IRS is reflected towards the ith MU, and the downlink rate of the ith MU can be expressed as

$$R_i^{IRS} = \log_2(1+\alpha_i+\beta_i) + \log_2(1+\alpha_j). \tag{35}$$

As far as the IOS-assisted communication system is concerned, on the other hand, the downlink rate can be expressed as

$$R_i^{IOS} = \log_2(1+\alpha_i+\frac{\beta_i}{\epsilon+1}) + \log_2(1+\alpha_j+\frac{\epsilon\beta_i}{\epsilon+1}). \tag{36}$$

Given the value of α_i, β_i, and α_j, R_i^{IOS} is a function of ϵ. The maximum value of R_i^{IOS} can be obtained by analyzing its derivate with respect to ϵ.

$$\frac{dR_i^{IOS}}{d\epsilon} = \frac{\beta_i(\alpha_i-\alpha_j)}{(\epsilon+1)^2} + \frac{\beta_i^2(1-\epsilon)}{(\epsilon+1)^3}, \tag{37a}$$

$$\frac{d^2R_i^{IOS}}{d\epsilon^2} = \frac{-2\beta_i\left((\alpha_i-\alpha_j-\beta_i^2)\epsilon+(\alpha_i-\alpha_j+2\beta_i^2)\right)}{(\epsilon+2)^4}. \tag{37b}$$

Without loss of generality, we assume that $\alpha_i \geq \alpha_j$. Since $\epsilon \in (0,1)$, we have $(\alpha_i-\alpha_j-\beta_i^2)\epsilon + (\alpha_i-\alpha_j+2\beta_i^2) \in (\alpha_i-\alpha_j+2\beta_i^2, 2\alpha_i-2\alpha_j+\beta_i^2)$. Given that $\alpha_i-\alpha_j+2\beta_i^2 > 0$ and $2\alpha_i-2\alpha_j+\beta_i^2 > 0$, the value of $(\alpha_i-\alpha_j-\beta_i^2)\epsilon + (\alpha_i-\alpha_j+2\beta_i^2)$ is larger than 0. Therefore, we have $\frac{d^2R_i^{IOS}}{d\epsilon^2} < 0$, which shows that R_i^{IOS} is a concave function, and the maximum value is obtained for $\epsilon^{opt} = \frac{\alpha_i-\alpha_j+\beta_i}{\alpha_j-\alpha_i+\beta_i}$. When we substitute ϵ^{opt} into (36), the maximum rate is given by $R_i^{IOS,opt} = \log_2\left(1+\alpha_i+\alpha_j+\frac{\alpha_i\alpha_j}{2}+\frac{\alpha_i^2}{4}+\frac{\alpha_j^2}{4}+\beta_i+\frac{\beta_i(\alpha_i+\alpha_j)}{2}+\frac{\beta_i^2}{4}\right)$. When comparing the value of $R_i^{IOS,opt}$ with R_i^{IRS} multiplied by a factor of two, we have

$$\begin{aligned} 2R_i^{IRS} &= \log_2(1+\alpha_i+\beta_i)^2(1+\alpha_j)^2 \\ &> \log_2\left(1+\alpha_i+\alpha_j+\frac{\alpha_i\alpha_j}{2}+\frac{\alpha_i^2}{4}+\frac{\alpha_j^2}{4}+\beta_i \right. \\ &\quad \left. +\frac{\beta_i(\alpha_i+\alpha_j)}{2}+\frac{\beta_i^2}{4}\right) = R_i^{IOS,opt}. \end{aligned} \tag{38}$$

On the other hand, when $\alpha_i \to 0$, $\alpha_j \to 0$, and $\beta_i \to \infty$, we have

$$\frac{R_i^{IOS,opt}}{R_i^{IRS}} \to 2. \tag{39}$$

Combining (38) and (39), we conclude that the ratio of the downlink sum-rate of an IOS-assisted system and an IRS-assisted system is upper-bounded by two. This concludes the proof.

REFERENCES

[1] Ericsson White Paper, "More than 50 billion connected devices," Utah Education Network, Salt Lake City, UT, USA, Tech. Rep. 284 23-3149, Feb. 2011.

[2] D. Wang, Y. Zhang, H. Wei, X. You, X. Gao, and J. Wang, "An overview of transmission theory and techniques of large-scale antenna systems for 5G wireless communications," *Sci. China Inf. Sci.*, vol. 59, no. 081301, pp. 1–18, Aug. 2016.

[3] A. Gatherer. (Jun. 2018). *What Will 6G Be*. [Online]. Available: https://www.comsoc.org/publications/ctn/what-will-6g-be

[4] Huawei. (Sep. 2019). *Asia–Pacific Leads 5G Innovation, Huawei Enables Sustainable Development of a Digital Economy*. [Online]. Available: https://www.huawei.com/en/press-events/news/2019/9/huawei-5th-asia-pacific-innovation-day

[5] S. Zhang, H. Zhang, B. Di, and L. Song, "Cellular UAV-to-X communications: Design and optimization for multi-UAV networks," *IEEE Trans. Wireless Commun.*, vol. 18, no. 2, pp. 1346–1359, Jan. 2019.

[6] P. Yang, M. Di Renzo, Y. Xiao, S. Li, and L. Hanzo, "Design guidelines for spatial modulation," *IEEE Commun. Surveys Tuts.*, vol. 17, no. 1, pp. 6–26, 1st Quart. 2015.

[7] E. G. Larsson, O. Edfors, F. Tufvesson, and T. L. Marzetta, "Massive MIMO for next generation wireless systems," *IEEE Commun. Mag.*, vol. 52, no. 2, pp. 186–195, Feb. 2014.

[8] S. Gong *et al.*, "Towards smart wireless communications via intelligent reflecting surfaces: A contemporary survey," *IEEE Commun. Surveys Tuts.*, vol. 22, no. 4, pp. 2283–2341, 4th Quart., 2020.

[9] Q. Li, M. Wen, and M. Di Renzo, "Single-RF MIMO: From spatial modulation to metasurface-based modulation," 2020, *arXiv:2009.00789*. [Online]. Available: http://arxiv.org/abs/2009.00789

[10] J. G. Andrews *et al.*, "What will 5G be?" *IEEE J. Sel. Areas Commun.*, vol. 32, no. 6, pp. 1065–1082, Jun. 2014.

[11] M. Di Renzo *et al.*, "Smart radio environments empowered by reconfigurable ai meta-surfaces: An idea whose time has come," *EURASIP J. Wireless Commun. Netw.*, vol. 2019, no. 1, pp. 1–20, 2019.

[12] H. Hashida, Y. Kawamoto, and N. Kato, "Intelligent reflecting surface placement optimization in air-ground communication networks toward 6G," *IEEE Wireless Commun.*, vol. 27, no. 6, pp. 146–151, Dec. 2020.

[13] M. Di Renzo *et al.*, "Reconfigurable intelligent surfaces vs. Relaying: Differences, similarities, and performance comparison," *IEEE Open J. Commun. Soc.*, vol. 1, pp. 798–807, Jun. 2020.

[14] L. Li *et al.*, "Enhanced reconfigurable intelligent surface assisted mmWave communication: A federated learning approach," *China Commun.*, vol. 17, no. 10, pp. 115–128, Oct. 2020.

[15] M. A. El Mossallamy, H. Zhang, L. Song, K. G. Seddik, Z. Han, and G. Y. Li, "Reconfigurable intelligent surfaces for wireless communications: Principles, challenges, and opportunities," *IEEE Trans. Cogn. Commun. Netw.*, vol. 6, no. 3, pp. 990–1002, Sep. 2020.

[16] M. D. Renzo *et al.*, "Smart radio environments empowered by reconfigurable intelligent surfaces: How it works, state of research, and road ahead," *IEEE J. Sel. Areas Commun.*, vol. 38, no. 11, pp. 2450–2525, Nov. 2020.

[17] Y. Liu *et al.*, "Reconfigurable intelligent surfaces: Principles and opportunities," 2020, *arXiv:2007.03435*. [Online]. Available: http://arxiv.org/abs/2007.03435

[18] X. Qian, M. Di Renzo, J. Liu, A. Kammoun, and M.-S. Alouini, "Beamforming through reconfigurable intelligent surfaces in single-user MIMO systems: SNR distribution and scaling laws in the presence of channel fading and phase noise," *IEEE Wireless Commun. Lett.*, vol. 10, no. 1, pp. 77–81, Jan. 2021.

[19] W. Yan, X. Yuan, Z.-Q. He, and X. Kuai, "Passive beamforming and information transfer design for reconfigurable intelligent surfaces aided multiuser MIMO systems," *IEEE J. Sel. Areas Commun.*, vol. 38, no. 8, pp. 1793–1808, Aug. 2020.

[20] L. Li *et al.*, "Machine-learning reprogrammable metasurface imager," *Nature Commu.*, vol. 10, no. 1, pp. 1–8, 2019.

[21] H. Zhang, H. Zhang, B. Di, K. Bian, Z. Han, and L. Song, "Towards ubiquitous positioning by leveraging reconfigurable intelligent surface," *IEEE Commun. Lett.*, vol. 25, no. 1, pp. 284–288, Jan. 2021.

[22] J. Hu *et al.*, "Reconfigurable intelligent surfaces based radio-frequency sensing: Design, optimization, and implementation," *IEEE J. Sel. Areas Commun.*, vol. 38, no. 11, pp. 2700–2716, Nov. 2020.

[23] C. Huang *et al.*, "Holographic MIMO surfaces for 6G wireless networks: Opportunities, challenges, and trends," *IEEE Wireless Commun.*, vol. 27, no. 5, pp. 118–125, Oct. 2020.

[24] H.-T. Chen, A. J. Taylor, and N. Yu, "A review of metasurfaces: Physics and applications," *Rep. Prog. Phys.*, vol. 79, no. 7, Jun. 2016, Art. no. 076401.
[25] G. C. Alexandropoulos and E. Vlachos, "A hardware architecture for reconfigurable intelligent surfaces with minimal active elements for explicit channel estimation," in *Proc. IEEE Int. Conf. Acoust., Speech Signal Process. (ICASSP)*, May 2020, pp. 9175–9179.
[26] N. Shlezinger, G. C. Alexandropoulos, M. F. Imani, Y. C. Eldar, and D. R. Smith, "Dynamic metasurface antennas for 6G extreme massive MIMO communications," *IEEE Wireless Commun.*, vol. 28, no. 2, pp. 106–113, Apr. 2021.
[27] C. Huang, A. Zappone, G. C. Alexandropoulos, M. Debbah, and C. Yuen, "Reconfigurable intelligent surfaces for energy efficiency in wireless communication," *IEEE Trans. Wireless Commun.*, vol. 18, no. 8, pp. 4157–4170, Aug. 2019.
[28] H. L. Zhang, B. Y. Di, L. Y. Song, and Z. Han, "Reconfigurable intelligent surfaces assisted communications with limited phase shifts: How many phase shifts are enough?" *IEEE Trans. Veh. Technol.*, vol. 69, no. 4, pp. 4498–4502, Apr. 2020.
[29] X. Yu, D. Xu, and R. Schober, "MISO wireless communication systems via intelligent reflecting surfaces," in *Proc. IEEE ICCC*, Changchun, China, Aug. 2019, pp. 735–740.
[30] C. Pan *et al.*, "Multicell MIMO communications relying on intelligent reflecting surfaces," *IEEE Trans. Wireless Commun.*, vol. 19, no. 8, pp. 5218–5233, Aug. 2020.
[31] NTT DOCOMO. (Jan. 2020). *DOCOMO Conducts World's First Successful Trial of Transparent Dynamic Metasurface*. [Online]. Available: https://www.nttdocomo.co.jp/english/info/media_center/pr/2020/0117_00.html
[32] F. H. Danufane, M. Di Renzo, J. De Rosny, and S. Tretyakov, "On the path-loss of reconfigurable intelligent surfaces: An approach based on Green's theorem applied to vector fields," *IEEE Trans. Commun.*, early access, May 17, 2021, doi: 10.1109/TCOMM.2021.3081452.
[33] S. Zhang, H. Zhang, B. Di, Y. Tan, Z. Han, and L. Song, "Beyond intelligent reflecting surfaces: Reflective-transmissive metasurface aided communications for full-dimensional coverage extension," *IEEE Trans. Veh. Technol.*, vol. 69, no. 11, pp. 13905–13909, Nov. 2020.
[34] T. Cai, G. Wang, J. Liang, Y. Zhuang, and T. Li, "High-performance transmissive meta-surface for C-/X-band lens antenna application," *IEEE Trans. Antennas Propag.*, vol. 65, no. 7, pp. 3598–3606, Jul. 2017.
[35] S. Zeng *et al.*, "Reconfigurable intelligent surfaces in 6G: Reflective, transmissive, or both?" *IEEE Commun. Lett.*, vol. 25, no. 6, pp. 2063–2067, Jun. 2021.
[36] M. L. N. Chen, L. J. Jiang, and W. E. I. Sha, "Detection of orbital angular momentum with metasurface at microwave band," *IEEE Antennas Wireless Propag. Lett.*, vol. 17, no. 1, pp. 110–113, Jan. 2018.
[37] B. Di, H. Zhang, L. Song, Y. Li, Z. Han, and H. V. Poor, "Hybrid beamforming for reconfigurable intelligent surface based multi-user communications: Achievable rates with limited discrete phase shifts," *IEEE J. Sel. Areas Commun.*, vol. 38, no. 8, pp. 1809–1822, Aug. 2020.
[38] V. Arun and H. Balakrishnan, "RFocus: Practical beamforming for small devices," 2019, *arXiv:1905.05130*. [Online]. Available: http://arxiv.org/abs/1905.05130
[39] D. M. Pozar, *Microwave Engineering*. New York, NY, USA: Wiley, 2005.
[40] A. Ishimaru, *Electromagnetic Wave Propagation, Radiation, and Scattering: From Fundamentals to Applications*. Hoboken, NJ, USA: Wiley, 2017.
[41] H. Rajabalipanah, M. Fallah, and A. Abdolali, "A fast, straightforward, and accurate computer-aided design for highly efficient metasurface–assisted Fabry–Perot cavity antennas based on the equivalent circuit approach," *AEU-Int. J. Electron. Commun.*, vol. 97, pp. 252–262, Dec. 2018.
[42] W. Tang *et al.*, "Wireless communications with reconfigurable intelligent surface: Path loss modeling and experimental measurement," *IEEE Trans. Wireless Commun.*, vol. 20, no. 1, pp. 421–439, Jan. 2021.
[43] C. Pfeiffer and A. Grbic, "Metamaterial Huygens' surfaces: Tailoring wave fronts with reflectionless sheets," *Phys. Rev. Lett.*, vol. 110, no. 197401, pp. 1–5, May 2013.
[44] D. Tse and P. Viswanath, *Fundamentals Wireless Communication*. Cambridge, U.K.: Cambridge Univ. Press, 2005.
[45] F. Rusek *et al.*, "Scaling up MIMO: Opportunities and challenges with very large arrays," *IEEE Signal Process. Mag.*, vol. 30, no. 1, pp. 40–60, Jan. 2013.
[46] S. Bubeck, "Convex optimization: Algorithms and complexity," 2014, *arXiv:1405.4980*. [Online]. Available: http://arxiv.org/abs/1405.4980
[47] B. Di, H. Zhang, L. Li, L. Song, Y. Li, and Z. Han, "Practical hybrid beamforming with finite-resolution phase shifters for reconfigurable intelligent surface based multi-user communications," *IEEE Trans. Veh. Technol.*, vol. 69, no. 4, pp. 4565–4570, Apr. 2020.

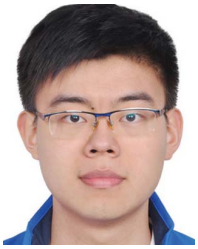

Shuhang Zhang (Student Member, IEEE) received the B.S. degree in electronic engineering from the School of Electrical Engineering and Computer Science, Peking University, Beijing, China, in 2016, where he is currently pursuing the Ph.D. degree. His current research interests include reconfigurable intelligent surface communication systems, unmanned aerial vehicle networks, cooperative communications, and non-orthogonal multiple access.

Hongliang Zhang (Member, IEEE) received the B.S. and Ph.D. degrees from the School of Electrical Engineering and Computer Science, Peking University, in 2014 and 2019, respectively. From July 2019 to July 2020, he was a Post-Doctoral Fellow with the Department of Electrical and Computer Engineering, University of Houston, Texas. He is currently a Post-Doctoral Associate with the Department of Electrical and Computer Engineering, Princeton University, NJ, USA. His current research interests include reconfigurable intelligent surfaces, aerial access networks, and game theory. He has served as a TPC Member for many IEEE conferences, such as Globecom, ICC, and WCNC. He received the Best Doctoral Thesis Award from the Chinese Institute of Electronics in 2019. He was a recipient of the 2021 IEEE Comsoc Heinrich Hertz Award for best communications letters. He is an Editor for *IET Communications* and *Frontiers in Signal Processing*. He also serves as a Guest Editor for IEEE INTERNET OF THINGS JOURNAL (IoT-J) Special Issue on Internet of UAVs over Cellular Networks. He is an Exemplary Reviewer for IEEE TRANSACTIONS ON COMMUNICATIONS in 2020.

Boya Di (Member, IEEE) received the B.S. degree in electronic engineering from Peking University, China, in 2014, and the Ph.D. degree from the Department of Electronics, Peking University, in 2019. She has been working as a Post-Doctoral Researcher with Imperial College London since August 2019, and currently works as an Assistant Professor at Peking University. Her current research interests include integrated aerial access and satellite networks, reconfigurable intelligent surfaces, multi-agent systems, edge computing, and vehicular networks. She has served as a TPC Member for GlobeCom 2016, GlobeCom 2020, ICCC 2017, ICC 2016, ICC 2018, ICC 2020, and VTC 2019. She has also been serving as an Associate Editor for IEEE TRANSACTIONS ON VEHICULAR TECHNOLOGY since June 2020.

Yunhua Tan received the Ph.D. degree from Peking University in 2003. In November 2006, he joined the Department of Electronics, School of Electronics Engineering and Computer Science, Peking University, where he is currently an Associate Professor. His main research interests include microwave, millimeter wave, terahertz electronics, and computational electromagnetics and its applications.

Marco Di Renzo (Fellow, IEEE) received the Laurea *(cum laude)* and Ph.D. degrees in electrical engineering from the University of L'Aquila, Italy, in 2003 and 2007, respectively, and the Habilitation à Diriger des Recherches (Doctor of Science) degree from University Paris-Sud (now Paris-Saclay University), France, in 2013. Since 2010, he has been with the French National Center for Scientific Research (CNRS), where he is currently the CNRS Research Director (a CNRS Professor) with the Laboratory of Signals and Systems (L2S), Paris-Saclay University–CNRS and CentraleSupelec, Paris, France. In Paris-Saclay University, he serves as the Coordinator of the Communications and Networks Research Area, Laboratory of Excellence DigiCosme, and as a member of the Admission and Evaluation Committee of the Ph.D. School on Information and Communication Technologies. He is a fellow of the U.K. Institution of Engineering and Technology (IET), an Ordinary Member of the European Academy of Sciences and Arts (EASA), and a member of the Academia Europaea (AE). He is also a highly cited researcher in 2019. He has received several research distinctions, which include the SEE-IEEE Alain Glavieux Award, the IEEE Jack Neubauer Memorial Best Systems Paper Award, the Royal Academy of Engineering Distinguished Visiting Fellowship, the Nokia Foundation Visiting Professorship, the Fulbright Fellowship, and the 2021 *EURASIP Journal on Wireless Communications and Networking* Best Paper Award. He is the Editor-in-Chief of IEEE COMMUNICATIONS LETTERS and a Distinguished Speaker of the IEEE Vehicular Technology Society. From 2017 to 2020, he was a Distinguished Lecturer of the IEEE Vehicular Technology Society and the IEEE Communications Society.

Zhu Han (Fellow, IEEE) received the B.S. degree in electronic engineering from Tsinghua University in 1997, and the M.S. and Ph.D. degrees in electrical and computer engineering from the University of Maryland at College Park, College Park, in 1999 and 2003, respectively.

From 2000 to 2002, he was an Research and Development Engineer with JDSU, Germantown, Maryland. From 2003 to 2006, he was a Research Associate with the University of Maryland. From 2006 to 2008, he was an Assistant Professor at Boise State University, Idaho. He is currently a John and Rebecca Moores Professor with the Department of Electrical and Computer Engineering and the Department of Computer Science, University of Houston, Texas. He is also a Chair Professor with National Chiao Tung University, ROC. His research interests include wireless resource allocation and management, wireless communications and networking, game theory, big data analysis, security, and smart grid. He received the NSF Career Award in 2010, the Fred W. Ellersick Prize of the IEEE Communication Society in 2011, the EURASIP Best Paper Award for the Journal on Advances in Signal Processing in 2015, IEEE Leonard G. Abraham Prize in the field of communications systems (Best Paper Award in IEEE JOURNAL ON SELECTED AREAS IN COMMUNICATIONS (JSAC)) in 2016, and several best paper awards in IEEE conferences. He is also the Winner of the 2021 IEEE Kiyo Tomiyasu Award for outstanding early to mid-career contributions to technologies holding the promise of innovative applications, with the following citation "for contributions to game theory and distributed management of autonomous communication networks." He is a 1% highly cited researcher since 2017 according to Web of Science. He is an IEEE Communications Society Distinguished Lecturer from 2015 to 2018.

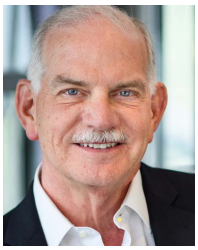

H. Vincent Poor (Life Fellow, IEEE) received the Ph.D. degree in electrical engineering and computer science (EECS) from Princeton University in 1977.

From 1977 to 1990, he was on the faculty of the University of Illinois at Urbana-Champaign. Since 1990, he has been on the faculty at Princeton University, where he is currently a Michael Henry Strater University Professor. From 2006 to 2016, he served as the Dean for Princeton's School of Engineering and Applied Science. He has also held visiting appointments at several other universities, including most recently at Berkeley and Cambridge. His research interests include the areas of information theory, signal processing, and machine learning, and their applications in wireless networks, energy systems, and related fields. Among his publications in these areas is the forthcoming book *Machine Learning and Wireless Communications* (Cambridge University Press, 2021). He is a member of the National Academy of Engineering and the National Academy of Sciences, and a foreign member of the Chinese Academy of Sciences, the Royal Society, and other national and international academies. Recent recognition of his work includes the 2017 IEEE Alexander Graham Bell Medal.

Lingyang Song (Fellow, IEEE) received the Ph.D. degree from the University of York, U.K., in 2007. He worked as a Post-Doctoral Research Fellow with the University of Oslo, Norway, and Harvard University, until rejoining Philips Research U.K. in March 2008. In May 2009, he joined the Department of Electronics, School of Electronics Engineering and Computer Science, Peking University, and is currently a Boya Distinguished Professor. He has coauthored four text books, including *Wireless Device-to-Device Communications and Networks* and *Full-Duplex Communications and Networks* (Cambridge University Press, U.K.). He has co-edited two books, such as *Orthogonal Frequency Division Multiple Access (OFDMA)-Fundamentals and Applications* and *Evolved Network Planning and Optimization for UMTS and LTE* (IEEE ComSoc Best Readings) (Auerbach Publications, CRC Press). His main research interests include cooperative and cognitive communications, physical layer security, and wireless *ad-hoc*/sensor networks. He has coauthored 16 Best Paper Awards and one Best Demo Award, including the IEEE Heinrich Hertz Award for Best Communications Letters Award in 2021, the IEEE Leonard G. Abraham Prize in 2016, the Best Paper Awards from the IEEE Communication Society Flagship Conference, such as IEEE ICC 2014, IEEE ICC 2015, IEEE Globecom 2014, and the Best Demo Award in the ACM Mobihoc 2015. He received the National Science Fund for Distinguished Young Scholars in 2017, the First Prize in the Nature Science Award of Ministry of Education of China in 2017, the National Science Fund for Excellent Young Scholars in 2013, and the IEEE Communications Society Asia Pacific (AP) Young Researcher Award in 2012. He received the K. M. Stott Prize for excellent research. He served as the TPC Co-Chair for ICUFN 2011/2012 and IEEE ICCC 2019. He served as the Symposium Co-Chair for IEEE ICC 2014/2016, IEEE VTC 2016 spring, and IEEE Globecom 2016. He has served as the Vice Chair for the IEEE Communications Society Cognitive Network Technical Committee since 2016 and the IEEE Communications Society Asia Pacific Board Technical Affairs Committee since 2016. He also serves as a Section Editor for *Handbook of Cognitive Radio* (Springer) since 2016. He has served as an Area Editor for the IEEE TRANSACTIONS ON VEHICULAR TECHNOLOGY since 2019, an Editor for IEEE TRANSACTIONS ON COMMUNICATIONS since 2019, *China Communications* since 2015, and IEEE TRANSACTIONS ON WIRELESS COMMUNICATIONS from 2013 to 2018. He has served as a Distinguished Lecturer for the IEEE Communications Society from 2015 to 2018.